Efficient Industrial Robot Calibration via a Novel Unscented Kalman Filter-Incorporated Variable Step-Size Levenberg–Marquardt Algorithm

Zhibin Li, Shuai Li, *Senior Member, IEEE*, and Xin Luo, *Senior Member, IEEE*

***Abstract*— Robots facilitate a critical category of equipment to implement intelligent production. However, due to extensively inevitable factors like structural errors and gear tolerances, the positioning error of an industrial robot is several millimeters, therefore failing to fulfill the high-precision manufacturing requirements. To address the critical problem, this work develops a novel calibration algorithm that incorporates an unscented Kalman filter and a variable step-size Levenberg–Marquardt (UKF-VSLM) algorithm for efficient industrial robot calibration with the following twofold ideas: 1) developing a novel variable step-size Levenberg–Marquardt (VSLM) algorithm to address the local optimum issues encountered by a standard Levenberg–Marquardt (LM) algorithm and 2) incorporating an unscented Kalman filter (UKF) into the proposed VSLM algorithm to suppressing the measurement noises during the calibration process. Empirical studies on a HuShu Robotics (HSR) JR680 industrial robot demonstrate that compared with state-of-the-art calibration algorithms, the calibration accuracy of the developed UKF-VSLM is 19.51% higher than that of the most accurate LM algorithm measured by the maximum error. The empirical results strongly support the superior performance of the proposed algorithm in addressing robot calibration issues.**

***Index Terms*— Absolute positioning accuracy, industrial robots, kinematic parameters, robot calibration, unscented Kalman filter (UKF), variable step-size Levenberg–Marquardt (VSLM).**

NOMENCLATURE

Symbol	Description.
K	Transformation matrix.
a	Link length: The distance from z_{i-1} to z_i axes.
d	Link offset: The distance from x_{i-1} to x_i axes.
α	Link twist angle: The angle from z_{i-1} to z_i axes.
θ	Joint angle: The angle from x_{i-1} to x_i axes.
$q_1, q_2, \ldots, q_6$	Rotation angles of an industrial robot.
J	Robot coefficient matrix.
Z_i	Measuring cable length for the position i.
Z'_i	Theoretical cable length for the position i.
P_i	Theoretical position for the position i.
P_0	Calculated position for the point fixed on the ground.
X	Errors of DH parameters.
dK	Pose deviation of the end-effector.
e	Position error of the end-effector.
E	Cable length deflection.
$X'_{i,k\|k-1}$	Posteriori sigma vector at $(k-1)$th iteration.
$Y'_{i,k\|k-1}$	Posteriori measurement state $(k-1)$th iteration.
P_k^-	Covariance matrix at time k.
$\hat{x}_k^-$	Priori state at time k.
W_i	Weight of sigma point i.
δ	Step size of searching.
$\hat{y}$	Mean of the observation model.
S	Covariance of the observation model.
ρ	Kalman gain.
m	Number of samples.
P_{xy}	Cross-covariance.
Y_k	Current set of observations at the kth iteration.
λ	Learning rate.
$\|\|\cdot\|\|_2$	L_2norm operator.
$f(\cdot)$	Fitness function.
μ	Decreasing coefficient of step size.
I	Unit matrix.

Manuscript received 27 January 2023; revised 10 March 2023; accepted 23 March 2023. Date of publication 10 April 2023; date of current version 26 April 2023. This work was supported in part by the National Natural Science Foundation of China under Grant 62272078 and in part by the Chinese Association for Artificial Intelligence (CAAI)-Huawei MindSpore Open Fund under Grant CAAIXSJLJJ-2021-035A. The Associate Editor coordinating the review process was Dr. Gabriele Patrizi. *(Corresponding authors: Shuai Li; Xin Luo.)*

Zhibin Li and Xin Luo are with the College of Computer and Information Science, Southwest University, Chongqing 400715, China (e-mail: LiZhibin111@outlook.com; luoxin@swu.edu.cn).

Shuai Li is with the Faculty of Information Technology and Electrical Engineering, University of Oulu, 90570 Oulu, Finland, and also with the VTT-Technical Research Centre of Finland, 90590 Oulu, Finland (e-mail: shuai.li@oulu.fi).

Digital Object Identifier 10.1109/TIM.2023.3265744

I. INTRODUCTION

INDUSTRIAL robots are the major equipment of advanced manufacture. The vigorous development of industrial robotics can help the fast establishment of advanced manufacture [1], [2], [3], [4], [5], which further promotes industrial upgrading to improve people's daily life. However, industrial robot applications commonly involve complex tasks with high precision requirements [5], [6], [7], [8], [9], [10]. Generally, a calibrated industrial robot enjoys its greatly high repetitive positioning accuracy, while the absolute

This work is licensed under a Creative Commons Attribution 4.0 License. For more information, see https://creativecommons.org/licenses/by/4.0/

positioning error of an uncalibrated robot might reach several millimeters and thus fail the demands of high-precision offline programming and intelligent application [11], [15], [18]. Additionally, the error sources of industrial robots mainly contain robot kinematic and dynamic errors, where the kinematic parameter error yields about 90% of the total errors [11], [12], [13], [14], [15]. Hence, we mainly consider the error of robot kinematic parameters. Consequently, implementing its kinematic parameter calibration efficiently is a vital method to enhance the positioning accuracy of the robot [16], [17], [18], [19], [20].

Aiming at addressing the thorny issue of robot calibration, pioneer researchers have made various explorations [21], [22], [23], [24], [25]. Liu et al. [1] design a closed-loop kinematic calibration method with a six-point measuring device, which adopts the Levenberg–Marquardt (LM) algorithm to calibrate a UR10 robot. Xu et al. [2] propose an improved manta ray foraging optimization algorithm for calibrating a self-designed 6-DOF robot, which reduces the robot positioning error from 10.24 to 0.55 mm. Cao et al. [3] incorporate an extended Kalman filter (EKF) into an artificial neural network (ANN) with a butterfly and flower pollination algorithm for calibrating the Stewart platform, which achieves excellent calibration performance. Wang et al. [5] develop a beetle swarm optimization-incorporated multilayer neural network model for calibration. Experiments on a SIASUN SR210D robot manipulator demonstrate that this calibrator achieves fast convergence and high calibration accuracy. Chen and Zhan [4] develop an improved beetle swarm optimization algorithm to calibrate a KUKA KR500L340-2 robot, thereby obviously reducing its positioning error. The above-mentioned calibration methods all are able to improve the robot calibration accuracy. However, they frequently suffer from the issue of falling into the local optimum, which harms the calibration accuracy.

As analyzed in a prior study, there are extensive measurement noises in robot calibration, which results in this terrible phenomenon. Moreover, the stationary step size of an LM algorithm may also limit its optimization ability when seeking the optimal kinematic parameters. Motivated by the above discovery, this article proposes an efficient robot calibration algorithm based on an unscented Kalman filter (UKF) algorithm and a newly presented variable step-size Levenberg–Marquardt (VSLM) algorithm. Specifically, the ideas of this work are threefold.

1) Incorporating the variable step-size term into the learning scheme of an LM algorithm, thereby achieving a VSLM algorithm with high searching stability and computing efficiency.
2) Adopting a UKF to suppress the measurement noises.
3) Building a calibration algorithm via seamlessly cascading a UKF and a VSLM, which can efficiently discover the optimal kinematic parameters of the robot.

The major contributions of this work include the following.

1) This article proposes a novel VSLM algorithm with variable step size, which achieves better searching ability than a standard LM algorithm.
2) A UKF-VSLM calibration algorithm is proposed to achieve efficient and accurate industrial robot calibration results.
3) Detailed algorithm design and analysis for the developed UKF-VSLM calibrator have been provided, which provide essential guidance for researchers and practitioners.
4) Empirical studies on a HuShu Robotics (HSR) JR680 industrial robot demonstrate that compared with state-of-the-art calibration algorithms, the calibration accuracy of the developed UKF-VSLM is 19.51% higher than that of the most accurate LM algorithm measured by the maximum error.

TABLE I
KINEMATIC PARAMETERS OF THE HSR JR680 ROBOT BEFORE CALIBRATION

Item i	α_i/°	a_i/mm	d_i/mm	θ_i/°
1	-90	250	653.5	0
2	0	900	0	-90
3	90	-205	0	180
4	-90	0	1030.2	0
5	90	0	0	90
6	0	0	200.6	0

II. PROBLEM STATEMENT

First, this work discusses the kinematic model and error model for the industrial robot, and then the principle of calibration algorithm based on a drawstring displacement sensor is discussed. Furthermore, the adopted symbols are depicted in Nomenclature.

To accurately optimize the robot kinematic parameter errors, this work carefully gathers the robot position data [26], [27], [28], [29], [30]. Advanced measuring instruments like a laser tracker, a theodolite, and a vision device are either very expensive or lead to low calibration efficiency [31], [32], [33], [34], [35]. Meanwhile, they mostly require particular maintenance, which further restricts their industrial applications in real environments [36], [37], [38], [39], [40]. Hence, for simulating real industrial needs, we adopt a drawstring displacement sensor as the data-gathering instrument [41], [42], [43], [44], [45]. It contains the virtues of high measurement accuracy and stability as well as convenience [45], [46], [47], [48], [49], [50].

Note that robot calibration has four parts: 1) kinematic modeling; 2) measuring the position of the end-effector; 3) the identification of kinematic parameters; and 4) kinematic parameter errors compensation [51], [52], [53], [54], [55]. The modeling step hugely affects the industrial robot positioning error. Recently, the popular kinematic model is the DH (Denavit and Hartenberg) model. Hence, we adopt it to build the robot kinematic model. For an HSR JR680 industrial robot with six degrees of freedom, its joint angles and initial DH parameters are depicted in Fig. 1 and Table I, respectively.

For the principle of the classical DH model [54], [55], [56], [57], [58], [59], [60], the kinematic transformation of its adjacent joints is given as

$$K_i = \begin{bmatrix} \cos\theta_i & -\sin\theta_i\cos\alpha_i & \sin\theta_i\sin\alpha_i & a_i\cos\theta_i \\ \sin\theta_i & \cos\theta_i\cos\alpha_i & -\cos\theta_i\sin\alpha_i & a_i\sin\theta_i \\ 0 & \sin\alpha_i & \cos\alpha_i & d_i \\ 0 & 0 & 0 & 1 \end{bmatrix} \tag{1}$$

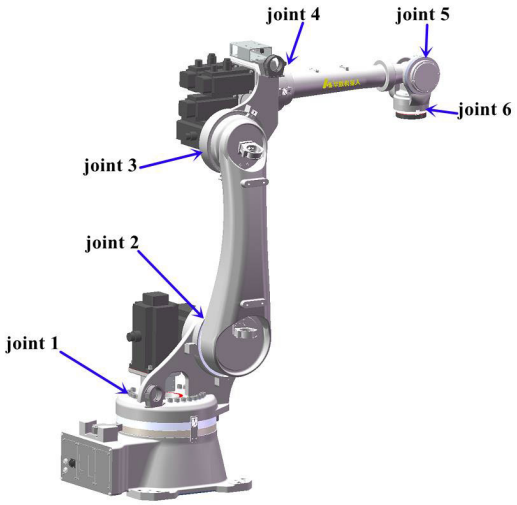

Fig. 1. Joints of the HSR JR680 industrial robot.

where K is the link transformation matrix, a_i represents the link length, d_i is the link offset, θ_i is defined as the joint angle, α_i is given the link twist angle [61], [62], [63], [64], [65]. So, the transformation relationship from the robot base to its end-effector is written as

$$K_6^0 = K_1^0 K_2^1 K_3^2 K_4^3 K_5^4 K_6^5. \tag{2}$$

To identify the DH parameters errors of the robot, the deviation of the robotic transformation matrix is calculated by

$$dK = K_R - K_6^0 \tag{3}$$

where dK represents the pose deviation of the robot and K_R is the actual pose of the robot. Based on (3), dK can be written as

$$dK_i = \frac{\partial K_i}{\partial \alpha_i} d\alpha_i + \frac{\partial K_i}{\partial a_i} da_i + \frac{\partial K_i}{\partial d_i} dd_i + \frac{\partial K_i}{\partial \theta_i} d\theta_i. \tag{4}$$

Based on (3) and (4), the pose error of the robot is represented as

$$e = \begin{bmatrix} J_1 & J_2 & J_3 & J_4 \end{bmatrix} \begin{bmatrix} \Delta a \\ \Delta d \\ \Delta \alpha \\ \Delta \theta \end{bmatrix} = JX \tag{5}$$

where J represents the differential identification Jacobian matrix and X represents the errors of the DH parameters.

Based on the robot calibration principle [66], [67], [68], [69], [70], the error of cable length is approximately equal to the robot positioning error, thus yielding the following learning function:

$$f(X) = \min \left[\frac{1}{m} \sum_{i=1}^{m} \left(Z_i - Z_i' \right)^2 \right] \tag{6}$$

where Z_i' and Z_i are the calculated cable length and measuring cable length, respectively, and m is the sampling point count.

Commonly, the nominal cable length can be calculated as

$$Z_i' = \sqrt{(P_i - P_0)^2}. \tag{7}$$

Note that P_i represents the calculated position of the robot end-effector and P_0 is defined as the coordinate value of the fixed point.

In general, the robot error model is a highly nonlinear model with extensively complex factors [71], [72], [73], [74], [75], whose analytic solutions cannot be achieved via conventional optimization algorithms. In addition, there are extensive measurement noises during the calibration process, which has huge harm to the robot positioning accuracy. To deal with this thorny problem, we propose an efficient UKF-VSLM algorithm to calibrate the robot.

III. UKF-VSLM Algorithm

A. UKF Algorithm

To address the estimation issue in nonlinear systems, a UKF algorithm is proposed by researchers. It adopts an unscented transformation to sample state values, whose average value and covariance are calculated by some sigma points. Compared with the linearization of the nonlinear system by the EKF, the UKF algorithm makes a higher approximation. Moreover, the UKF algorithm has been widely utilized in electronics, medical science, aerospace, and other fields [12].

First, considering the principle of the UKF algorithm, the sigma vector is addressed by the unscented transformation. Then the posteriori sigma vector $X'_{i,k|k-1}$ and the posteriori measuring state $Y'_{i,k|k-1}$ are presented as

$$\begin{cases} X'_{i,k|k-1} = \Phi_k \left(X'_{i,k-1} \right) \\ Y'_{i,k|k-1} = H_k \left(X'_{i,k|k-1} \right). \end{cases} \tag{8}$$

Based on (8), we can achieve the covariance P_k^- and priori state $\hat{x}_k^-$, where W_i is the weight of sigma point i

$$\begin{cases} \hat{x}_k^- = \sum_{i=0}^{N+1} W_i X'_{i,k|k-1} \\ P_k^- = \sum_{i=0}^{N+1} W_i \left(X'_{i,k|k-1} - \hat{x}_k^- \right) \left(X'_{i,k|k-1} - \hat{x}_k^- \right)^T. \end{cases} \tag{9}$$

Then the mean $\hat{y}$ and covariance S of the observation model are written as

$$\begin{cases} \hat{y}_{k|k-1} = \sum_{i=0}^{N+1} W_i Y'_{i,k|k-1} \\ S_{k|k-1} = \sum_{i=0}^{N+1} W_i \left(Y'_{i,k|k-1} - \hat{y}_{k|k-1} \right) \left(Y'_{i,k|k-1} - \hat{y}_{k|k-1} \right)^T. \end{cases} \tag{10}$$

Additionally, the Kalman gain ρ and the cross-covariance P_{xy} can be represented as

$$\begin{cases} P_{xy,k|k-1} = \sum_{i=0}^{N+1} W_i \left(X'_{i,k|k-1} - \hat{x}_k^- \right) \left(Y'_{i,k|k-1} - \hat{y}_{k|k-1} \right)^T, \\ \rho = P_{xy,k|k-1} S_{k|k-1}^{-1}. \end{cases} \tag{11}$$

Lastly, the updating estimation of X and the covariance P_k are as follows:

$$\begin{cases} \hat{x}_k = \hat{x}_{k|k-1}^- + \rho \left(Y_k - \hat{y}_{k|k-1} \right) \\ P_k = P_{k|k-1}^- - \rho S_{k|k-1} \rho^T \end{cases} \tag{12}$$

where Y_k represents the current set of observations.

B. VSLM Algorithm

Considering the robot error identification model (5), if the identification coefficient matrix J is a full-rank matrix, then the least-squares solution of robot calibration is obtained as

$$X = \left(J^T J\right)^{-1} \cdot J^T \cdot E \tag{13}$$

where $E = Z_i - Z_i'$.

However, the robot error model has redundant parameters, making J frequently suffers from singulars. Hence, the LM algorithm is adopted to address this issue, leading to the following solution:

$$X = \left(J^T J + \lambda I\right)^{-1} \cdot J^T \cdot E \tag{14}$$

where λ represents the learning rate and I represents the unit matrix. However, from (13), we see that the update of X is conducted with a stationary step size of one, which limits its searching ability. To address this issue, we incorporate a variable step size into its update rule as

$$\begin{cases} X = \left(J^T J + \lambda I\right)^{-1} \cdot J^T \cdot E \cdot \delta_t \\ \delta_{t+1} = \delta_t \cdot \mu \end{cases} \tag{15}$$

where δ is the step size of searching commonly set at 0.8, and the decaying constant μ lies in the (0, 1) interval and is commonly set at 0.95. Note that with (15), the step size keeps decreasing as the iteration count increases, thereby leading to the following effects: 1) at the early stage of objective minimization, the step size is large to make the model fast approach an equilibrium point and 2) as the training process continues, the step size gradually decreases to implement fine-tuning of the calibration model.

To make the convergence analysis of the developed VSLM algorithm, the meaningful theorem is presented as follows.

Theorem 1: As $f'(X) = 0$, if the initial kinematic parameters X_0 and coefficient matrix J_k developed by the Newton-like algorithm can satisfy the following equation:

$$\begin{cases} \left\| J_0^{-1} \right\| \le \beta \\ \left\| J_0^{-1} f'(X_0) \right\| \le \kappa \\ \| J_M - J_N \| \le \tau \| X_M - X_N \| \quad \forall X_M, X_N \in U(X_0, \xi). \end{cases} \tag{16}$$

If the convergence factor g satisfies the following conditions:

$$\begin{cases} g & = \beta\kappa\tau \le \dfrac{1}{2} \\ \xi & \ge 1 - \dfrac{\sqrt{1-2g}}{g\kappa} \end{cases} \tag{17}$$

where β, κ, and τ are the real numbers. Consequently, the equation $f'(X) = 0$ can achieve solutions in the range $U(X_0, \xi)$. Note that Jacobian matrix J_k should satisfy the Lipschitz condition in Theorem 1.

Proof of Theorem **1***:* The definition of a quadratic optimal function is given as

$$h(x) = \frac{1}{2}\tau x^2 - \frac{1}{\beta}x + \frac{\kappa}{\beta} = 0. \tag{18}$$

Let $h(x) = 0$, we achieve two roots

$$\begin{aligned} x^* &= \frac{1 - \sqrt{1 - 2\beta\tau\kappa}}{\beta\tau} \\ x^{**} &= \frac{1 + \sqrt{1 - 2\beta\tau\kappa}}{\beta\tau}. \end{aligned} \tag{19}$$

Based on (17), (19) can be reformulated as

$$\begin{aligned} x^* &= \frac{1 - \sqrt{1 - 2g}}{g}\kappa \\ x^{**} &= \frac{1 + \sqrt{1 - 2g}}{g}\kappa. \end{aligned} \tag{20}$$

Note that x_k is the solution of the Newton iteration sequence, and we have

$$x_{k+1} = x_k - \frac{h(x_k)}{h'(x_k)}. \tag{21}$$

According to [67] and [70], we can easily prove that $x_k \to x^*$. Then we should prove the following inequality:

$$\left\| \Delta X^* - \Delta X_k \right\| \le x^* - x_k \tag{22}$$

where ΔX the variation of kinematic parameters. According to [69], we can prove that

$$\| \Delta X_M - \Delta X_N \| \le x_M - x_N \quad \forall M, N \in R^* \tag{23}$$

where R^* is a positive integer. Due to the convergence of $\{x_k\}$, we can easily prove that $\{X_k\}$ is a Cauchy convergence sequence. Then we can obtain that the limits of the sequence $\{X_k\}$ are X^*.

Let $M \to \infty$, we achieve that $\| \Delta X^* - \Delta X_k \| \le x^* - x_k$.

Note that $\Delta X^* = 0$ and the continuity of $f'(X)$, we can achieve that $J^* = 0$. Therefore, X^* is the solution of equation $f'(X) = 0$. Most importantly, it is very vital to present the convergence analysis of the VSLM algorithm, which provides a theoretical basis for the proposed algorithm. Our theoretical proof is based on a Newton-like method, which also gives us some ideas to improve the algorithm in the future.

C. Calibration Process of a UKF-VSLM Algorithm

As discussed in Sections III-A and III-B, the UKF-VSLM algorithm consists of two parts: 1) adopting a UKF to address the thorny noises and 2)establishing a new VSLM algorithm to further search the optimal kinematic parameters of the robot. The flowchart of the developed UKF-VSLM algorithm is depicted in Fig. 2.

D. Algorithm Design and Analysis

According to the analysis of the developed Algorithm 1: UKF-VSLM, its time cost can be divided into three parts.

1) Initialization

$$T_{11} = \Theta(r) \tag{24}$$

where r is the dimension of X_0.

2) The time cost of the UKF step is

$$T_{12} = \Theta(T_3 \times M). \tag{25}$$

Algorithm 1 UKF-VSLM

Input: T_3, X_0, $\{q_{i,1}, q_{i,2}, \ldots, q_{i,6}\}$ $\{Y_1, Y_2, \ldots, Y_{|M|}\}$

	Operation	**Cost**
	/* Initialization */	
1	**Initialize** T_3, M, δ, μ, λ, T_9, W_i	T_{11}
2	**Initialize:** $X'_{i,k-1}$=X_0	
	/* Training Starts */	
	/* *UKF*-Step */	
3	**for** $k = 1$ **to** $\lvert T_3 \rvert$ **do**	
4	**set** $P_{(0)k}$ random number	
5	**set** $\rho_{(0)k}$ zero	
6	**for** $i = 1$ **to** $\lvert M \rvert$ **do**	
7	Update $X'_{i,k\lvert k-1}$, $Y'_{i,k\lvert k-1}$with (8)	
8	Calculate J_k with (5)	
9	Compute P_k^-, $\hat{x}_k^-$ based on (9)	T_{12}
10	Calculating $\hat{y}_{k\lvert k-1}$, $S_{k\lvert k-1}$ via (10)	
11	Updating $P_{xy,k\lvert k-1}$, ρ based on (11)	
12	Calculating $\hat{x}_k$, P_k with (12)	
13	**end for**	
14	**end for**	
15	$x_{ukf} = \hat{x}_k$	
	/* *VSLM*-Step */	
16	**for** $t = 1$ **to** $\lvert T_9 \rvert$ T_{13} **do**	
17	**set** $X_0 = x_{ukf}$	
18	**for** $i = 1$ **to** $\lvert M \rvert$ **do**	
19	Updating δ_{t+1}, X based on (15)	
20	**end for**	
21	**end for**	
	/* Operation Ending */	

Output: X

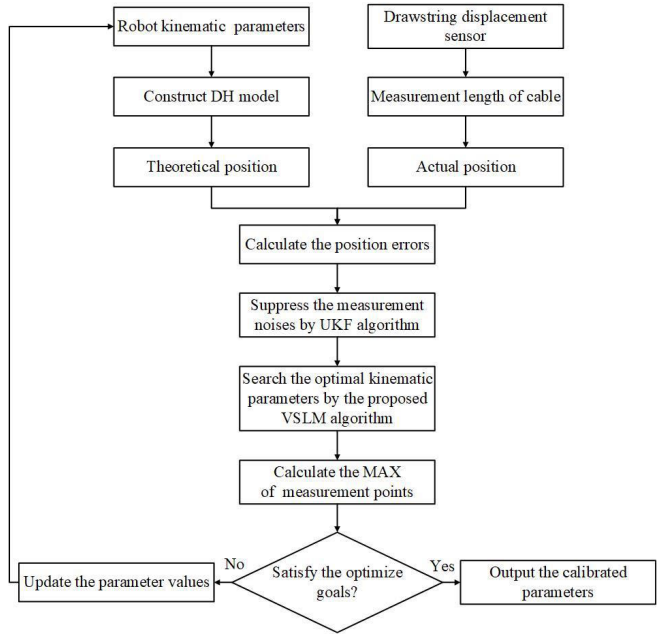

Fig. 2. Algorithm flowchart of robot error identification.

3) The time cost of the VSLM step is

$$T_{13} = \Theta(T_9 \times M). \tag{26}$$

Moreover, we commonly obtain $r \ll T_1 \times M$ in robot calibration, (24) is far less than $\Theta(T_1 \times M)$. Hence, the overall time cost of Algorithm UKF-VSLM is given as

$$T_1 = T_{11} + T_{12} + T_{13} \approx \Theta((T_3 + T_9) \times M). \tag{27}$$

Additionally, Algorithm 1 shows the detailed algorithm design of our proposed algorithm. T_3 and T_9 represent the maximum number of calculations for the UKF algorithm and VSLM algorithm, respectively. M represents the number of samples and X is the errors of DH parameters. Due to the measuring noises in robot calibration, the UKF algorithm is adopted to address this issue. Then the obtained parameter identification results by the UKF algorithm are taken as the input of the VSLM algorithm. Lastly, the optimal kinematic parameters are calculated by the VSLM algorithm [73], [74], [75], [76], [77], [78].

IV. Experimental Results

A. General Settings

1) Evaluation Metrics: In this part, the root mean squared error (RMSE), standard deviation (STD), and the maximum error (MAX) are utilized as the evaluation metrics

$$\begin{aligned} \text{MAX} &= \max\left\{\sqrt{(Z_i - Z'_i)^2}\right\}, \quad i = 1, 2, \ldots, m \\ \text{STD} &= \frac{1}{m}\sum_{i=1}^{m}\sqrt{(Z_i - Z'_i)^2} \\ \text{RMSE} &= \sqrt{\frac{1}{m}\sum_{i=1}^{m}(Z_i - Z'_i)^2}. \end{aligned} \tag{28}$$

2) Experimental Datasets: In this section, we collect three public datasets for our experiments, whose details are as follows.

1) D1: HSR-RobotCali. We collect 2000 samples on an HSR JR680 industrial robot, which are evenly distributed in the whole robot workspace. Then, Table II shows five samples of this dataset, each sample has six rotation angles and the measuring cable length. Lastly, we adopt the proposed method to accurately identify robot kinematic parameter errors. Moreover, this dataset is publicly available on the website.[1]
2) D2: RobotCali. It is collected by an ABB robot [75]. It has 1042 samples, each of which consists of the cable length and six rotation angles.[1] To conduct the robot calibration experiments, 120 sampling points are randomly selected from RobotCali.
3) D3: The public robot position dataset, which is gathered on the Universal Robot [65]. It contains 16 811 samples, which consist of four position datasets: A, B, C, and D. In addition, we choose 200 samples from A to conduct experiments.

Each dataset is implemented in 80%–20% train test settings.

[1]https://github.com/Lizhibing1490183152/HSR-RobotCali

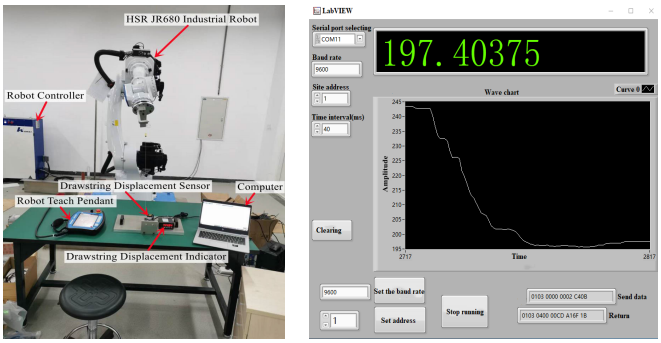

(a) (b)

Fig. 3. Robot calibration system. (a) Experimental devices consist of an HSR JR680 industrial robot, a drawstring displacement sensor, a teach pendant, and a computer. (b) Developed data-gathering software.

TABLE II
FIVE SAMPLES

No.	q1/◦	q2/◦	q3/◦	q4/◦	q5/◦	q6/◦	L/mm
1	1.41	-74.025	220.99	-166.357	41.989	65.122	350.07
2	10.14	-75.864	215.116	-177.022	37.363	65.125	365.28
3	8.146	-75.865	215.115	-177.022	37.363	65.125	351.77
4	2.76	-74.879	212.85	-177.943	41.991	65.124	389.07
5	9.998	-75.865	215.115	-177.022	37.363	65.125	364.54

TABLE III
SPECIFICATIONS OF THE DRAWSTRING DISPLACEMENT SENSOR HY150-2000

Item	Specification
Signal output type	Digital signal
Supply voltage	DC 5-24V
Measuring range	2000 mm
Maximum speed	1000m/s
Extension force	5N
Linearity	0.05% FS
Resolution	0.004mm
Operating temperature	-25℃～+85℃

TABLE IV
SPECIFICATIONS OF THE DRAWSTRING DISPLACEMENT INDICATOR HY9648

Item	Specification
Supply voltage	AC220V 50Hz
Input resistance	5K
Pulse frequency	⩽500K
Magnification range	0.000～999.999
Display range	-199999～999999
Pulse width	2us
Operating temperature	-10℃～50℃

3) Experimental Platform: To accurately calibrate the robot, we design an experimental platform as shown in Fig. 3(a). The HSR JR680 industrial robot produced by HuaShu robot company is used as an experimental subject. Then the position of the robotic end-effector is measured by a drawstring displacement sensor. Additionally, a drawstring displacement indicator is adopted for displaying the value of cable length. We have added the details of the utilized hardware in Tables III–V, including the drawstring displacement sensor, the drawstring displacement indicator, and HSR JR680 industrial robot. Moreover, MATLAB software is applied in dealing with this data and outputting the calibrated kinematic parameters.

TABLE V
SPECIFICATIONS OF THE HSR JR680 INDUSTRIAL ROBOT

Item	Specification
Degree of freedom	6
specified load	80Kg
Maximum working radius	2200.4mm
Repeatability	±0.07mm
rated power	6kW
Rated voltage	3 phaseAC380V
Rated current	10.8A
Body weight	722kg
Control cabinet weight	180KG
Control cabinet protection grade	IP53

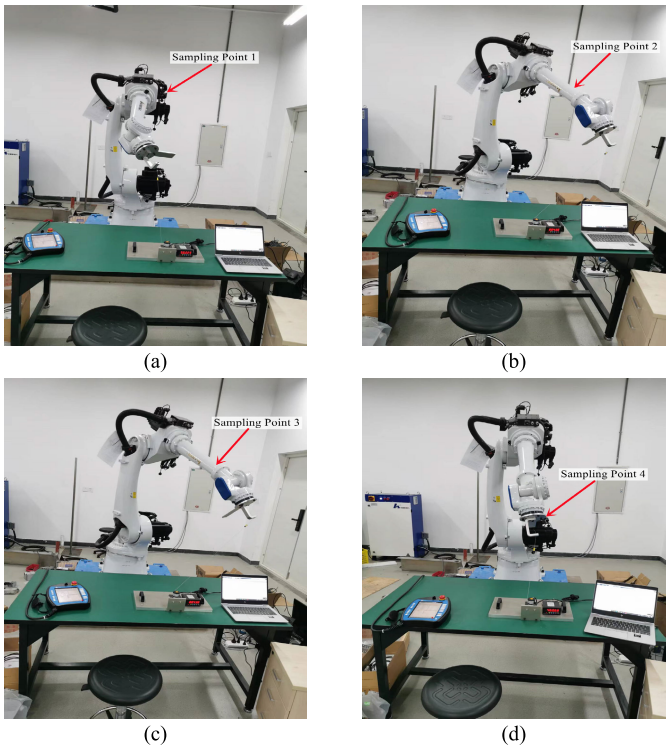

(a) (b) (c) (d)

Fig. 4. Data-gathering process of four samples. The data-gathering process is from sampling points 1–4, four diversified samples are gathered in different positions, which are adopted to calculate the robot positioning error. (a) Robot measuring pose for sampling point 1. (b) Robot measuring pose for sampling point 2. (c) Robot measuring pose for sampling point 3. (d) Robot measuring pose for sampling point 4.

4) Experimental Process: In the robot calibration process, to collect accurate samples, the selection of measurement points should cover the workspace of the HSR JR680 industrial robot. Fig. 4 shows the data-gathering process of four sampling points. In this work, 120 position points are chosen in the motion range of an HSR JR680 industrial robot, then a drawstring displacement sensor is utilized to measure the position of these sampling points. Furthermore, a data acquisition program is developed based on the LabVIEW software, which can conveniently record sample information. The developed program is shown in Fig. 3(b).

In this experiment, a training dataset with 100 samples is utilized to calculate the robot position error, then the remaining 20 samples are utilized as comparison data. After calibration, we compare the calibration accuracy of some state-of-the-art calibration algorithms to validate the correctness of the developed algorithm.

TABLE VI
COMPARED CALIBRATION ALGORITHMS

Algorithm	Description
M1	The conventional extended Kalman filter is adopted to address the measuring noise in calibration process by Jiang *et al*. [9].
M2	The beetle antennae search algorithm is proposed by Khan *et al*. [6], which is adopted to optimize robot trajectory.
M3	The unscented Kalman filter is developed in [12], which is adopted to reckon the errors of the robotic kinematic parameters.
M4	The particle swarm optimization algorithm is proposed by Lee *et al*. [37], which is also utilized to optimize robotic kinematic parameters.
M5	The Radial basis function neural network (RBF) proposed in [15], which is adopted to estimate the positional errors of target positions.
M6	The Levenberg-Marquardt (LM) algorithm proposed in [1], which is utilized to calibrate the kinematic parameters of the UR10 robot.
M7	The differential evolution algorithm is proposed by Zhou *et al*. [17], which can also accurately calibrate the robot.
M8	The variable step-size Levenberg-Marquardt (VSLM) algorithm, which enhances the calibration accuracy of LM algorithm by adding the variable step-size term.
M9	The proposed UKF-VSLM algorithm in this work, which can enhance the robot calibration performance.

TABLE VII
COMPUTATIONAL COMPLEXITY OF VARIOUS ALGORITHMS

Algorithm	Computational Complexity
M1	$\Theta(T_1 \times M)$
M2	$\Theta(T_2 \times M)$
M3	$\Theta(T_3 \times M)$
M4	$\Theta(T_4 \times M)$
M5	$\Theta(T_5 \times M)$
M6	$\Theta(T_6 \times M)$
M7	$\Theta(T_7 \times M)$
M8	$\Theta(T_8 \times M)$
M9	$\Theta((T_3+T_9) \times M)$

B. Comparison With Advanced Calibration Algorithms

In this part, we compare the calibration performance of the developed algorithm against several advanced algorithms. Table VI summarizes the details of all test algorithms. Table VII lists the computational complexity analyses of compared algorithms, which rely on the maximum number of iterations and the number of samples. T_1–T_9 are the maximum number of calculations for M1–M9, respectively. M denotes the number of samples. Table VIII lists the experimental results of various algorithms, then Table IX shows the iteration time cost of algorithms M1–M9. In addition, Table X shows the experimental results of the Wilcoxon signed-ranks test on RMSE/STD/MAX of Table VIII, and Table XI presents the experimental results of the Wilcoxon signed-ranks test on total time cost of Table IX. Moreover, Table XII shows the parameter errors identified by M9 on D1–D3, and Table XIII lists the parameter errors identified by M1–M9 on D1.

Fig. 5 shows the calibration results of various algorithms. Fig. 6 shows the training curves and the number of iterations rounds. Fig. 7 shows the robot calibration error of various algorithms on D1. Based on the above analysis, we summarize as follows.

1) **Compared with state-of-the-art calibration algorithms, the proposed UKF-VSLM algorithm has the best calibration accuracy.** As shown in Fig. 5(a) and Table VIII, M9 achieves the MAX error at 0.99 mm, which is, respectively, 38.89% lower than M1's 1.62 mm, 44.07% lower than M2's 1.77 mm, 35.71% lower than M3's 1.54 mm, 24.42% lower than M4's 1.31 mm, 48.70% lower than M5's 1.93 mm, 19.51% lower than M6's 1.23 mm, 34.43% lower than M7's 1.51 mm, 13.91% lower than M8's 1.15 mm on D1. Similar results are also encountered on D1–D3 when adopting RMSE and STD as the evaluation metrics, as shown in Figs. 5(a)–(c) and Table VIII.
2) **Incorporating variable step-size terms into the LM algorithm can enhance computational efficiency.** From Fig. 6(a) and (b), M8's converge rate is faster than that of M6. It only takes 20 iterations to reach the termination condition. We also obtain similar results on D2–D3, as illustrated in Table IX.
3) **The UKF-VSLM's time cost is higher than that of the most efficient calibration algorithms.** As depicted in Fig. 6(c) and Table IX, M9's time cost is lower than that of M2, M4, M6, and M7, but generally higher than that of M1, M3, M5, and M8. This is because the UKF-VSLM algorithm relies on a cascade structure, its UKF and VSLM components should be trained in a serial way for identifying robotic kinematic parameter errors. Note that such time costs can be greatly reduced by implementing efficient model parallelization with the help of GPU or other parallelization computing frameworks.
4) **The proposed UKF-VSLM algorithm obtains the best calibration performance among state-of-the-art calibration algorithms.** To accurately calibrate the robot, we adopt M9 to identify the kinematic parameters. Table XII shows the parameter errors identified by M9 on D1–D3, which can be adopted to compensate for the robot's kinematic parameters. Then, we utilize the calibrated kinematic parameters to calculate the M9's calibration accuracy on D1–D3. Moreover, Table XIII lists the parameter errors identified by M1–M9 on D1, which can be adopted to compensate kinematic parameters of the HSR JR680 industrial robot. Additionally, 2000 measurement points are obtained on an HSR JR680 industrial robot. After finishing the robot calibration, we compare the calibration results of these algorithms on D1, which is shown in Fig. 7. From the results, the robot positioning error is significantly reduced after calibration. M9 has the best calibration performance among M1–M8. Similar experiments are achieved on D2–D3, as shown in Table VIII.
5) **The accuracy gain of the proposed UKF-VSLM algorithm is significant.** We adopt the Wilcoxon signed-ranks test to check the effectiveness of the proposed algorithm in terms of calibration accuracy and total time cost when compared with other calibration algorithms, which is shown in Tables X and XI. Moreover, the Wilcoxon signed-ranks test consists of R+, R-, and p-value. The higher R+ represents the higher calibration accuracy and lower time cost, and the p-value is at

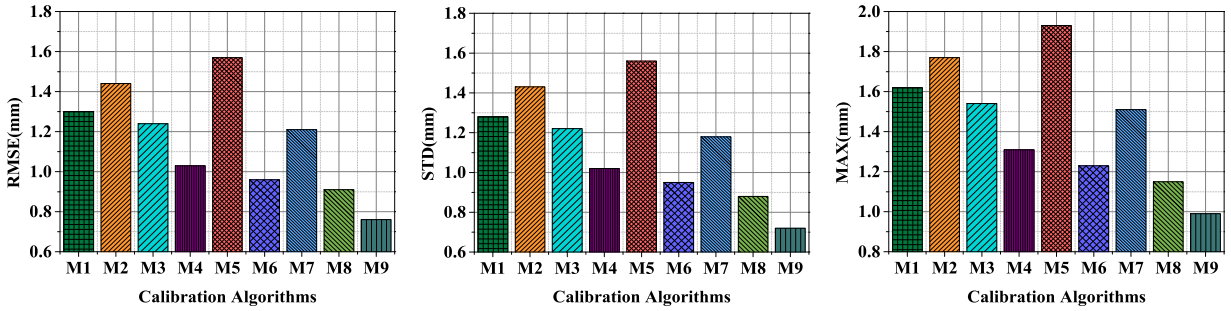

Fig. 5. Robot positioning accuracy of compared algorithms on D1. (a) RMSE. (b) Error STD. (c) Maximum error.

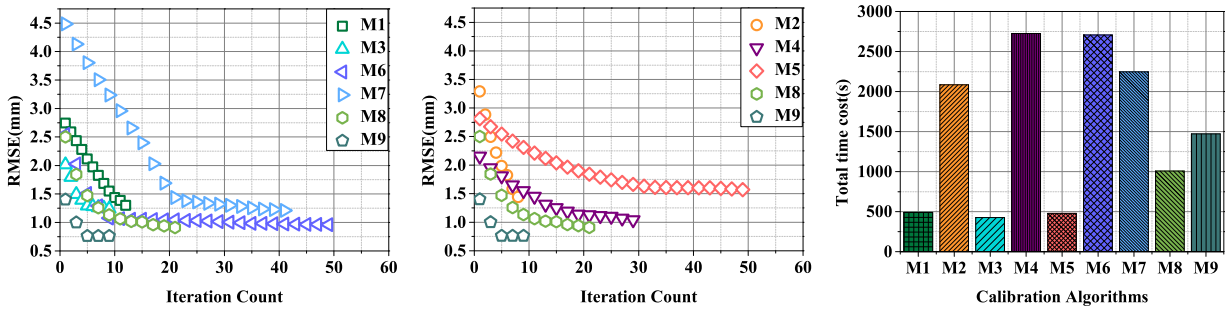

Fig. 6. Time cost and iteration curves of various calibration algorithms on D1. (a) M1, M3, and M6–M9. (b) M2, M4, M5, M8, and M9. (c) Total time cost of M1–M9.

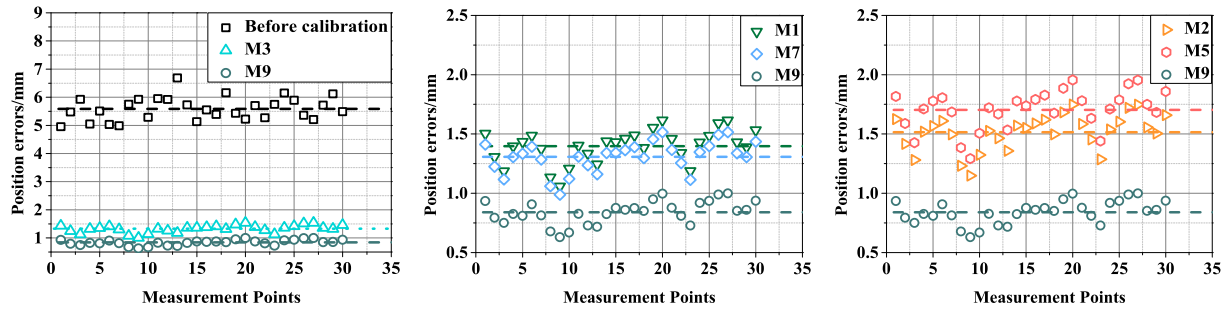

Fig. 7. Robot calibration error of various algorithms on D1. We evidently see that the developed calibration algorithm achieves the best calibration accuracy than other state-of-the-art algorithms. (a) Position errors of before calibration, M3, M9. (b) Position errors of M1, M7, M9. (c) Position errors of M2, M5, M9.

TABLE VIII

PERFORMANCE COMPARISON OF VARIOUS ALGORITHMS

Datasets	Metric(mm)	Before	M1	M2	M3	M4	M5	M6	M7	M8	M9
D1	RMSE	5.80	1.30	1.44	1.24	1.03	1.57	0.96	1.21	0.91	**0.76**
	STD	5.78	1.28	1.43	1.22	1.02	1.56	0.95	1.18	0.88	**0.72**
	MAX	6.83	1.62	1.77	1.54	1.31	1.93	1.23	1.51	1.15	**0.99**
D2	RMSE	2.09	0.66	0.7	0.64	0.59	0.85	0.50	0.67	0.45	**0.43**
	STD	2.00	0.56	0.56	0.55	0.49	0.72	0.41	0.58	0.36	**0.35**
	MAX	3.36	1.71	1.76	1.51	1.28	1.91	1.16	1.59	1.13	**1.05**
D3	RMSE	2.73	1.30	0.63	1.64	0.99	1.37	0.52	1.57	0.50	**0.48**
	STD	2.72	1.27	0.56	1.63	0.96	1.29	0.50	1.55	0.47	**0.44**
	MAX	3.09	2.33	1.58	1.98	1.47	2.46	0.89	2.29	0.86	**0.81**

TABLE IX

TOTAL ITERATION TIME OF M1–M9 ON RMSE

Datasets	Item	M1	M2	M3	M4	M5	M6	M7	M8	M9
D1	Iteration	12	8	9	30	400	60	40	20	**2**
	Time(s)	492.31	2084.62	427.61	2724.61	478.31	2707.21	2248.21	1008.16	**1471.20**
D2	Iteration	13	7	8	30	400	60	40	20	**2**
	Time(s)	24.96	108.69	23.85	137.79	24.18	135.12	123.16	50.59	**74.41**
D3	Iteration	14	20	12	50	250	50	50	16	**2**
	Time(s)	70.81	141.21	108.72	438.11	117.21	220.12	220.94	112.35	**224.31**

TABLE X

EXPERIMENTAL RESULTS OF WILCOXON SIGNED-RANKS TEST ON RMSE/STD/MAX OF TABLE VIII

Comparison	R+	R-	p-value*
M9 vs. M1	45	0	0.002
M9 vs. M2	45	0	0.002
M9 vs. M3	45	0	0.002
M9 vs. M4	45	0	0.002
M9 vs. M5	45	0	0.002
M9 vs. M6	45	0	0.002
M9 vs. M7	45	0	0.002
M9 vs. M8	45	0	0.002

*The highlighted significance level of accepted hypotheses is 0.05.

TABLE XI

RESULTS OF THE WILCOX ON SIGNED-RANKS TEST ON TOTAL TIME COST OF TABLE IX

Comparison	R+	R-	p-value*
M9 vs. M1	6	15	0.8438
M9 vs. M2	16	5	0.1563
M9 vs. M3	6	15	0.8438
M9 vs. M4	21	0	0.0156
M9 vs. M5	12	9	0.4063
M9 vs. M6	20	1	0.0313
M9 vs. M7	20	1	0.0313
M9 vs. M8	6	15	0.8438

*The highlighted significance level of accepted hypotheses is 0.05.

TABLE XII

IDENTIFIED DEVIATIONS OF KINEMATIC PARAMETERS THROUGH M9 ON D1–D3

Dataset	Joint i	$\Delta\alpha_i$/°	Δa_i/mm	Δd_i/mm	$\Delta\theta_i$/°
D1	1	0.0269	0.4844	0.7634	0.0184
	2	0.0466	-2.2899	0.6757	0.0796
	3	0.0178	0.3950	-0.1619	-0.0037
	4	0.0526	-0.5009	1.4994	0.0199
	5	-0.0648	3.6568	0.6200	-0.0571
	6	-0.1759	-1.4166	0.7177	-0.0092
D2	1	0.4495	-6.0598	4.2883	-0.2779
	2	0.0086	-3.1342	-2.7294	-0.2300
	3	-0.086	-0.3817	4.9957	-0.0808
	4	-0.0194	-0.2381	2.8729	-0.0937
	5	0.0925	-4.2741	1.4856	-0.1881
	6	-0.2402	-0.2200	2.2480	-0.0670
D3	1	0.0793	-1.9647	-0.3430	-0.0909
	2	0.0496	0.0698	2.2868	0.0367
	3	-0.0171	-2.8880	-1.5088	-0.0220
	4	0.0834	-1.3467	-0.5454	0.0507
	5	-0.0365	1.9816	0.5378	-0.1305
	6	-0.0249	-3.1609	-0.1984	-0.0068

the significance level. On the one hand, compared with M1–M8, M9 has the highest calibration accuracy. On the other hand, M9 has a higher significance than M4, M6, and M7 in terms of time cost. However, the unacceptable hypothesis emerges on M1–M3, M5, and M8, the reasons for which are given in Section IV-B.

C. Summary

From the above extensive experimental results, we can achieve the following summaries.

1) Generally speaking, laser tracker, theodolite, and vision devices are adopted for measuring the robot's position, which have high measurement accuracy. However, they have extremely complex operations and expensive prices. Meanwhile, to operate conveniently the instruments, we spend extensive time and energy training some professional engineers. Moreover, it is necessary to deal with the complex conversion operation between the robotic coordinate system and the coordinate system of measuring devices. To address this issue, we develop a measurement scheme with a drawstring displacement sensor, which has the advantages of good stability, convenient handling, small mass, low cost, and high measurement accuracy.

TABLE XIII

IDENTIFIED DEVIATIONS OF KINEMATIC PARAMETERS THROUGH M1–M9 ON D1

Algorithm	Joint i	$\Delta\alpha_i$/°	Δa_i/mm	Δd_i/mm	$\Delta\theta_i$/°
M1	1	0.1446	1.2214	-1.8888	0.0473
	2	0.0374	0.5151	-0.1057	0.0499
	3	0.1411	0.0462	2.6921	0.0636
	4	0.0145	0.5551	1.1547	0.0059
	5	-0.2016	1.8453	0.3933	0.1030
	6	-0.1753	0.7386	-1.1767	0.0349
M2	1	-0.0572	-0.3985	-1.3938	0.0192
	2	0.1999	-0.8359	-1.3797	-0.0415
	3	-0.0419	1.7630	1.2909	-0.2101
	4	0.0216	2.4466	2.0826	0.0060
	5	0.0857	2.0151	0.4554	-0.0080
	6	0.1173	-0.3495	0.9171	-0.0079
M3	1	-0.0457	4.7013	-1.1127	-0.0466
	2	-0.1819	-1.2524	3.1366	-0.1551
	3	-0.0030	-2.4222	-2.3075	-0.0941
	4	0.0465	1.3493	-0.3069	0.0520
	5	-0.0407	1.0722	0.7840	0.1081
	6	-0.0281	1.3286	0.3284	-0.0056
M4	1	0.0468	-0.6981	-0.3023	0.0014
	2	-0.1067	-0.5111	1.4879	0.1785
	3	-0.1361	-0.1107	-1.1048	-0.1162
	4	0.1607	0.8056	0.4056	-0.0642
	5	0.1966	0.9025	-1.3980	-0.1043
	6	0.0184	0.8444	0.3544	0.1630
M5	1	0.1128	1.4357	-0.6121	-0.0520
	2	-0.0299	-3.4737	0.1629	0.0334
	3	-0.0083	0.9905	0.2835	-0.1242
	4	0.0769	0.2021	0.4576	0.0983
	5	-0.0101	1.7463	-2.3814	0.1520
	6	0.0866	-0.8277	1.2687	0.0214
M6	1	-0.0494	2.0081	-0.6037	0.1334
	2	-0.0082	-0.0926	0.3088	-0.0274
	3	0.1774	1.9887	0.5615	0.1006
	4	0.0312	0.0569	0.0851	0.0410
	5	-0.0434	-2.9583	-1.4201	-0.0084
	6	0.1001	3.7408	3.1094	0.1178
M7	1	0.0654	-2.3757	-2.5023	0.1072
	2	0.2196	0.5540	-2.3722	0.1452
	3	-0.0034	-2.5583	-1.8929	0.1224
	4	-0.0888	0.3204	-1.6355	-0.0380
	5	0.2525	1.7129	0.5857	-0.0265
	6	-0.1292	1.4330	2.1255	0.0110
M8	1	0.0045	2.8232	-0.5238	0.0373
	2	0.0271	-0.2749	-0.1027	0.0027
	3	-0.0697	1.0944	-0.1999	0.0393
	4	-0.1028	-2.5508	1.2320	-0.1017
	5	0.0202	3.3996	-0.5407	-0.0520
	6	0.0021	-2.3639	-0.1818	-0.1183
M9	1	0.0269	0.4844	0.7634	0.0184
	2	0.0466	-2.2899	0.6757	0.0796
	3	0.0178	0.3950	-0.1619	-0.0037
	4	0.0526	-0.5009	1.4994	0.0199
	5	-0.0648	3.6568	0.6200	-0.0571
	6	-0.1759	-1.4166	0.7177	-0.0092

2) To improve the searching ability of the LM algorithm, the variable step-size term is incorporated into its learning rule. The proposed VSLM algorithm has high computational efficiency and calibration accuracy.
3) Based on the VSLM algorithm, we propose the UKF-VSLM algorithm to calibrate the robot. First, the UKF algorithm is employed to reduce the influence of measuring noises, then the VSLM algorithm is applied to further optimize the robot positioning error. Furthermore, it achieves best calibration accuracy than other advanced algorithms.
4) For the developed measurement scheme and the proposed calibration algorithm, we design the detailed experimental platform for robot calibration and complete its own assembly. Meanwhile, the software for this experiment is developed, which implements the proposed calibration algorithm. Last, the feasibility of the developed algorithm is verified by numerous experimental results.

V. Conclusion

To achieve high calibration accuracy, this work proposes a novel calibration algorithm combining a UKF algorithm and a VSLM algorithm. First, a UKF algorithm is adopted to optimize DH parameter errors, which addresses the issue of measuring noise in the calibration process. To improve the searching ability of the LM algorithm, a variable step-size term is incorporated into its evaluation rule. Then we propose a VSLM algorithm, which is utilized to further calibrate the robot position errors. Furthermore, the experimental results demonstrate that the developed UKF-VSLM algorithm achieves best calibration accuracy than other advanced algorithms. Therefore, the virtues of the proposed calibration method are as follows.

1) The UKF algorithm successfully addresses the issue of measuring noise in the calibration process.
2) The proposed VSLM algorithm can accelerate the convergence rate of the LM algorithm.
3) Based on the VSLM algorithm, the UKF-VSLM algorithm is proposed in this work, whose calibration accuracy is higher than other advanced algorithms.
4) The proposed calibration method with a drawstring displacement sensor significantly reduces the cost of the measurement instrument.

However, the proposed calibration method also has several defects.

1) In general, the proposed UKF-VSLM algorithm has high calibration accuracy. However, it suffers from computational efficiency loss when compared with the single UKF or VSLM algorithm.
2) This utilized calibration algorithm only considers the effect of geometric factors on robot positioning error, while it ignores the nongeometric factors, such as gear backlash and exterior load that may cause degeneration in robot positioning accuracy.
3) The proposed calibration algorithm is based on offline calibration calling for stopping the robot when performing the calibration, which affects the real industrial production process.

Aiming at addressing the above-mentioned issues, the future work is as follows.

1) We plan to design a model parallelization with the help of GPU or other parallelization computing frameworks for accelerating the proposed UKF-VSLM algorithm.
2) Nongeometric factors will be taken into account in modeling to obtain more accurate error sources.
3) Vision is a simple measurement method [76], which is able to conduct online calibration without stopping the robot. It also has the virtues of low cost, high accuracy, and high security. Therefore, we will develop a novel calibration method based on visual measurement equipment.
4) A neural network is an intelligent algorithm with strong robustness, independent learning ability, and high self-adaptability [2], [4], [78], which can approximate any continuous nonlinear function. Hence, it is also appropriate for addressing the issue of robot calibration. In a word, we plan to develop a state-of-the-art calibration algorithm with a neural network to improve robot positioning accuracy.
5) With the complexity of the robot application environment, higher industrial requirements are put forward for the robot. To satisfy the complex measurement environment, we plan to design a new measurement method with various spatial constraints, like plane constraints and point constraints.

References

[1] Y. Liu, Z. Zhuang, and Y. Li, "Closed-loop kinematic calibration of robots using a six-point measuring device," *IEEE Trans. Instrum. Meas.*, vol. 71, pp. 1–12, 2022.
[2] X. Xu et al., "A novel calibration method for robot kinematic parameters based on improved manta ray foraging optimization algorithm," *IEEE Trans. Instrum. Meas.*, vol. 72, pp. 1–11, 2023.
[3] H. Cao, H. Nguyen, T. Tran, H. Tran, and J. Jeon, "A robot calibration method using a neural network based on a butterfly and flower pollination algorithm," *IEEE Trans. Ind. Electron.*, vol. 69, no. 4, pp. 3865–3875, Apr. 2022.
[4] X. Chen and Q. Zhan, "The kinematic calibration of an industrial robot with an improved beetle swarm optimization algorithm," *IEEE Robot. Autom. Lett.*, vol. 7, no. 2, pp. 4694–4701, Apr. 2022.
[5] Y. Wang, Z. Chen, H. Zu, X. Zhang, C. Mao, and Z. Wang, "Improvement of heavy load robot positioning accuracy by combining a model-based identification for geometric parameters and an optimized neural network for the compensation of nongeometric errors," *Complexity*, vol. 2020, Jan. 2020, Art. no. 5896813.
[6] A. T. Khan, S. Li, and X. Zhou, "Trajectory optimization of 5-link biped robot using beetle antennae search," *IEEE Trans. Circuits Syst. II, Exp. Briefs*, vol. 68, no. 10, pp. 3276–3280, Oct. 2021.
[7] J. Santolaria, F.-J. Brosed, J. Velázquez, and R. Jiménez, "Self-alignment of on-board measurement sensors for robot kinematic calibration," *Precis. Eng.*, vol. 37, no. 3, pp. 699–710, Jul. 2013.
[8] C. Fan, G. Zhao, J. Zhao, L. Zhang, and L. Sun, "Calibration of a parallel mechanism in a serial-parallel polishing machine tool based on genetic algorithm," *Int. J. Adv. Manuf. Technol.*, vol. 81, nos. 1–4, pp. 27–37, May 2015.
[9] Z. H. Jiang, W. G. Zhou, H. Li, Y. Mo, W. C. Ni, and Q. Huang, "A new kind of accurate calibration method for robotic kinematic parameters based on the extended Kalman and particle filter algorithm," *IEEE Trans. Ind. Electron.*, vol. 65, no. 4, pp. 3337–3345, Apr. 2018.
[10] P. Bai, J. Mei, T. Huang, and D. G. Chetwynd, "Kinematic calibration of delta robot using distance measurements," *Proc. Inst. Mech. Eng. C, J. Mech. Eng. Sci.*, vol. 230, no. 3, pp. 414–424, Feb. 2016.
[11] Z. Fu, J. S. Dai, K. Yang, X. Chen, and P. López-Custodio, "Analysis of unified error model and simulated parameters calibration for robotic machining based on lie theory," *Robot. Comput.-Integr. Manuf.*, vol. 61, Feb. 2020, Art. no. 101855.

[12] G. Du, Y. Liang, C. Li, P. X. Liu, and D. Li, "Online robot kinematic calibration using hybrid filter with multiple sensors," *IEEE Trans. Instrum. Meas.*, vol. 69, no. 9, pp. 7092–7107, Sep. 2020.

[13] N. Yu, R. Yang, and M. Huang, "Deep common spatial pattern based motor imagery classification with improved objective function," *Int. J. Netw. Dyn. Intell.*, vol. 1, no. 1, pp. 73–84, Dec. 2022.

[14] K. Kamali and I. A. Bonev, "Optimal experiment design for elasto-geometrical calibration of industrial robots," *IEEE/ASME Trans. Mechatronics*, vol. 24, no. 6, pp. 2733–2744, Dec. 2019.

[15] D. Chen, T. Wang, P. Yuan, N. Sun, and H. Tang, "A positional error compensation method for industrial robots combining error similarity and radial basis function neural network," *Meas. Sci. Technol.*, vol. 30, no. 12, Sep. 2019, Art. no. 125010.

[16] L. Ma, P. Bazzoli, P. M. Sammons, R. G. Landers, and D. A. Bristow, "Modeling and calibration of high-order joint-dependent kinematic errors for industrial robots," *Robot. Comput.-Integr. Manuf.*, vol. 50, pp. 153–167, Apr. 2018.

[17] S. Zhou, L. Xing, X. Zheng, N. Du, L. Wang, and Q. Zhang, "A self-adaptive differential evolution algorithm for scheduling a single batch-processing machine with arbitrary job sizes and release times," *IEEE Trans. Cybern.*, vol. 51, no. 3, pp. 1430–1442, Mar. 2021.

[18] C. Li, Y. Wu, H. Löwe, and Z. Li, "POE-based robot kinematic calibration using axis configuration space and the adjoint error model," *IEEE Trans. Robot.*, vol. 32, no. 5, pp. 1264–1279, Oct. 2016.

[19] F. Bi, X. Luo, B. Shen, H. Dong, and Z. Wang, "Proximal alternating-direction-method-of-multipliers-incorporated nonnegative latent factor analysis," *IEEE/CAA J. Autom. Sinica*, early access, Mar. 28, 2023, doi: 10.1109/JAS.2023.123474.

[20] A. Joubair and I. A. Bonev, "Non-kinematic calibration of a six-axis serial robot using planar constraints," *Precis. Eng.*, vol. 40, pp. 325–333, Apr. 2015.

[21] R. B. Sousa, M. R. Petry, and A. P. Moreira, "Evolution of odometry calibration methods for ground mobile robots," in *Proc. IEEE Int. Conf. Auto. Robot Syst. Competitions (ICARSC)*. Azores, Portugal: Univ. of Azores, Apr. 2020, pp. 294–299.

[22] T. S. Lembono, F. Suárez-Ruiz, and Q.-C. Pham, "SCALAR: Simultaneous calibration of 2-D laser and robot kinematic parameters using planarity and distance constraints," *IEEE Trans. Autom. Sci. Eng.*, vol. 16, no. 4, pp. 1971–1979, Oct. 2019.

[23] W. Wang, F. Liu, and C. Yun, "Calibration method of robot base frame using unit quaternion form," *Precis. Eng.*, vol. 41, pp. 47–54, Jul. 2015.

[24] Z. Liu, X. Luo, and M. Zhou, "Symmetry and graph bi-regularized non-negative matrix factorization for precise community detection," *IEEE Trans. Autom. Sci. Eng.*, pp. 1–15, 2023, doi: 10.1109/TASE.2023.3240335.

[25] Y. Zhou, X. Luo, and M. Zhou, "Cryptocurrency transaction network embedding from static and dynamic perspectives: An overview," *IEEE/CAA J. Autom. Sinica*, vol. 10, no. 5, pp. 1–17, May 2023, doi: 10.1109/JAS.2023.123450.

[26] W. Tian, M. Mou, J. Yang, and F. Yin, "Kinematic calibration of a 5-DOF hybrid kinematic machine tool by considering the ill-posed identification problem using regularisation method," *Robot. Comput.-Integr. Manuf.*, vol. 60, pp. 49–62, Dec. 2019.

[27] Y. Jiang, T. Li, L. Wang, and F. Chen, "Kinematic error modeling and identification of the over-constrained parallel kinematic machine," *Robot. Comput.-Integr. Manuf.*, vol. 49, pp. 105–119, Feb. 2018.

[28] W. Yang, S. Li, Z. Li, and X. Luo, "Highly-accurate manipulator calibration via extended Kalman filter-incorporated residual neural network," *IEEE Trans. Ind. Informat.*, early access, Feb. 2, 2023, doi: 10.1109/TII.2023.3241614.

[29] T. Huang, D. Zhao, F. Yin, W. Tian, and D. G. Chetwynd, "Kinematic calibration of a 6-DOF hybrid robot by considering multicollinearity in the identification Jacobian," *Mechanism Mach. Theory*, vol. 131, pp. 371–384, Jan. 2019.

[30] G. Du and P. Zhang, "Online robot calibration based on vision measurement," *Robot. Comput.-Integr. Manuf.*, vol. 29, no. 6, pp. 484–492, Dec. 2013.

[31] G. Xiong, Y. Ding, L. M. Zhu, and C. Y. Su, "A product-of-exponential-based robot calibration method with optimal measurement configurations," *Int. J. Adv. Robot. Syst.*, vol. 14, no. 6, pp. 1–12, Nov. 2017.

[32] Y. Guo, S. B. Yin, Y. J. Ren, J. G. Zhu, S. R. Yang, and S. H. Ye, "A multilevel calibration technique for an industrial robot with parallelogram mechanism," *Precis. Eng.*, vol. 40, pp. 261–272, Apr. 2015.

[33] X. Luo, H. Wu, Z. Wang, J. Wang, and D. Meng, "A novel approach to large-scale dynamically weighted directed network representation," *IEEE Trans. Pattern Anal. Mach. Intell.*, vol. 44, no. 12, pp. 9756–9773, Dec. 2022.

[34] D. Wu, M. Shang, X. Luo, and Z. Wang, "An L_1-and-L_2-norm-oriented latent factor model for recommender systems," *IEEE Trans. Neural Netw. Learn. Syst.*, vol. 33, no. 10, pp. 5775–5788, Oct. 2021.

[35] J. Santolaria, J. Conte, M. Pueo, and C. Javierre, "Rotation error modeling and identification for robot kinematic calibration by circle point method," *Metrol. Meas. Syst.*, vol. 21, no. 1, pp. 85–98, Feb. 2014.

[36] J. F. Peng, Y. Ding, G. Zhang, and H. Ding, "An enhanced kinematic model for calibration of robotic machining systems with parallelogram mechanisms," *Robot. Comput.-Integr. Manuf.*, vol. 59, pp. 92–103, Oct. 2019.

[37] J. H. Lee, J.-Y. Song, D.-W. Kim, J.-W. Kim, Y.-J. Kim, and S.-Y. Jung, "Particle swarm optimization algorithm with intelligent particle number control for optimal design of electric machines," *IEEE Trans. Ind. Electron.*, vol. 65, no. 2, pp. 1791–1798, Feb. 2018.

[38] H. Zhong, C. Hu, X. Li, L. Gao, B. Zeng, and H. Dong, "Kinematic calibration method for a two-segment hydraulic leg based on an improved whale swarm algorithm," *Robot. Comput.-Integr. Manuf.*, vol. 59, pp. 361–372, Oct. 2019.

[39] L. Kong, G. Chen, Z. Zhang, and H. Wang, "Kinematic calibration and investigation of the influence of universal joint errors on accuracy improvement for a 3-DOF parallel manipulator," *Robot. Comput.-Integr. Manuf.*, vol. 49, pp. 388–397, Feb. 2018.

[40] X. Luo, Z. Liu, L. Jin, Y. Zhou, and M. Zhou, "Symmetric nonnegative matrix factorization-based community detection models and their convergence analysis," *IEEE Trans. Neural Netw. Learn. Syst.*, vol. 33, no. 3, pp. 1203–1215, Mar. 2022.

[41] H. Wu, X. Luo, and M. Zhou, "Advancing non-negative latent factorization of tensors with diversified regularization schemes," *IEEE Trans. Serv. Comput.*, vol. 15, no. 3, pp. 1334–1344, May/Jun. 2022.

[42] W. Wang, H. Song, Z. Yan, L. Sun, and Z. Du, "A universal index and an improved PSO algorithm for optimal pose selection in kinematic calibration of a novel surgical robot," *Robot. Comput.-Integr. Manuf.*, vol. 50, pp. 90–101, Apr. 2018.

[43] C. Mao, S. Li, Z. Chen, X. Zhang, and C. Li, "Robust kinematic calibration for improving collaboration accuracy of dual-arm manipulators with experimental validation," *Measurement*, vol. 155, Apr. 2020, Art. no. 107524.

[44] Z. Li, S. Li, and X. Luo, "An overview of calibration technology of industrial robots," *IEEE/CAA J. Autom. Sinica*, vol. 8, no. 1, pp. 23–36, Jan. 2021.

[45] S. He, L. Ma, C. Yan, C.-H. Lee, and P. Hu, "Multiple location constraints based industrial robot kinematic parameter calibration and accuracy assessment," *Int. J. Adv. Manuf. Technol.*, vol. 102, nos. 5–8, pp. 1037–1050, Jun. 2019.

[46] X. Shi, Q. He, X. Luo, Y. Bai, and M. Shang, "Large-scale and scalable latent factor analysis via distributed alternative stochastic gradient descent for recommender systems," *IEEE Trans. Big Data*, vol. 8, no. 2, pp. 420–431, Apr. 2022.

[47] W. Zhenhua, X. Hui, C. Guodong, S. Rongchuan, and L. Sun, "A distance error based industrial robot kinematic calibration method," *Ind. Robot, Int. J.*, vol. 41, no. 5, pp. 439–446, Aug. 2014.

[48] X. Chen, Q. Zhang, and Y. Sun, "Non-kinematic calibration of industrial robots using a rigid–flexible coupling error model and a full pose measurement method," *Robot. Comput.-Integr. Manuf.*, vol. 57, pp. 46–58, Jun. 2019.

[49] J. M. Ahola, T. Seppälä, J. Koskinen, and T. Heikkilä, "Calibration of the pose parameters between coupled 6-axis F/T sensors in robotics applications," *Robot. Auto. Syst.*, vol. 89, pp. 1–8, Mar. 2017.

[50] X. Luo, Z. Liu, M. Shang, J. Lou, and M. Zhou, "Highly-accurate community detection via pointwise mutual information-incorporated symmetric non-negative matrix factorization," *IEEE Trans. Netw. Sci. Eng.*, vol. 8, no. 1, pp. 463–476, Jan. 2021.

[51] X. Luo, Y. Yuan, S. Chen, N. Zeng, and Z. Wang, "Position-transitional particle swarm optimization-incorporated latent factor analysis," *IEEE Trans. Knowl. Data Eng.*, vol. 34, no. 8, pp. 3958–3970, Aug. 2022.

[52] F. Li, Q. Zeng, K. F. Ehmann, J. Cao, and T. Li, "A calibration method for overconstrained spatial translational parallel manipulators," *Robot. Comput.-Integr. Manuf.*, vol. 57, pp. 241–254, Jun. 2019.

[53] L. Wang and N. Simaan, "Geometric calibration of continuum robots: Joint space and equilibrium shape deviations," *IEEE Trans. Robot.*, vol. 35, no. 2, pp. 387–402, Apr. 2019.

[54] Z. Xie, P. Zong, P. Yao, and P. Ren, "Calibration of 6-DOF industrial robots based on line structured light," *Optik*, vol. 183, pp. 1166–1178, Apr. 2019.

[55] X. Luo, H. Wu, and Z. Li, "NeuLFT: A novel approach to nonlinear canonical polyadic decomposition on high-dimensional incomplete tensors," *IEEE Trans. Knowl. Data Eng.*, early access, May 20, 2022, doi: 10.1109/TKDE.2022.3176466.

[56] X. Luo, Y. Zhou, Z. Liu, and M. Zhou, "Fast and accurate non-negative latent factor analysis of high-dimensional and sparse matrices in recommender systems," *IEEE Trans. Knowl. Data Eng.*, vol. 35, no. 4, pp. 3897–3911, Apr. 2023, doi: 10.1109/TKDE.2021.3125252.

[57] Y. Su, H. Cai, and J. Huang, "The cooperative output regulation by the distributed observer approach," *Int. J. Netw. Dyn. Intell.*, vol. 1, no. 1, pp. 20–35, Dec. 2022.

[58] F. M. Shakiba, M. Shojaee, S. M. Azizi, and M. Zhou, "Real-time sensing and fault diagnosis for transmission lines," *Int. J. Netw. Dyn. Intell.*, vol. 1, no. 1, pp. 36–47, Dec. 2022.

[59] Y. Jiang, T. Li, L. Wang, and F. Chen, "Kinematic accuracy improvement of a novel smart structure-based parallel kinematic machine," *IEEE/ASME Trans. Mechatronics*, vol. 23, no. 1, pp. 469–481, Feb. 2018.

[60] F. Campisano et al., "Online disturbance estimation for improving kinematic accuracy in continuum manipulators," *IEEE Robot. Autom. Lett.*, vol. 5, no. 2, pp. 2642–2649, Apr. 2020.

[61] N. Zeng, P. Wu, Z. Wang, H. Li, W. Liu, and X. Liu, "A small-sized object detection oriented multi-scale feature fusion approach with application to defect detection," *IEEE Trans. Instrum. Meas.*, vol. 71, 2022, Art. no. 3507014.

[62] T. Chuthai, M. O. T. Cole, T. Wongratanaphisan, and P. Puangmali, "Adaptive kinematic mapping based on Chebyshev interpolation: Application to flexure-jointed micromanipulator control," *IEEE/ASME Trans. Mechatronics*, vol. 25, no. 1, pp. 118–129, Feb. 2020.

[63] J. He, Q. Ding, F. Gao, and H. Zhang, "Kinematic calibration methodology of hybrid manipulator containing parallel topology with main limb," *Measurement*, vol. 152, Feb. 2020, Art. no. 107334.

[64] S. Li, Z. Du, and H. Yu, "A robot-assisted spine surgery system based on intraoperative 2D fluoroscopy navigation," *IEEE Access*, vol. 8, pp. 51786–51802, 2020.

[65] C. Landgraf, K. Ernst, G. Schleth, M. Fabritius, and M. F. Huber, "A hybrid neural network approach for increasing the absolute accuracy of industrial robots," in *Proc. IEEE 17th Int. Conf. Autom. Sci. Eng. (CASE)*, Lyon, France, Aug. 2021, pp. 468–474.

[66] L. Li, H. Ding, and G. Wang, "Kinematics parameter identification and accuracy evaluation method for neurosurgical robot," *J. Biomed. Eng.*, vol. 36, no. 6, pp. 994–1002, Dec. 2019.

[67] A. R. Conn, N. I. M. Gould, and P. L. Toint, "Convergence of quasi-Newton matrices generated by the symmetric rank one update," *Math. Program.*, vol. 50, nos. 1–3, pp. 177–195, Mar. 1991.

[68] H. Wang, T. Gao, J. Kinugawa, and K. Kosuge, "Finding measurement configurations for accurate robot calibration: Validation with a cable-driven robot," *IEEE Trans. Robot.*, vol. 33, no. 5, pp. 1156–1169, Oct. 2017.

[69] Q. Sun, H. Chen, J. Yang, and J. Yang, "Analysis on convergence of Newton-like power flow algorithm," *Proc. CSEE*, vol. 34, no. 13, pp. 2196–2200, May 2014.

[70] J. Hao, G. Zhang, K. Yang, M. Wu, Y. Zheng, and W. Hu, "Online unified solution for selective harmonic elimination based on stochastic configuration network and Levenberg–Marquardt algorithm," *IEEE Trans. Ind. Electron.*, vol. 69, no. 10, pp. 10724–10734, Oct. 2022.

[71] C. Mao, Z. Chen, S. Li, and X. Zhang, "Separable nonlinear least squares algorithm for robust kinematic calibration of serial robots," *J. Intell. Robot. Syst.*, vol. 101, no. 1, pp. 1–12, Jan. 2021.

[72] Z. Li, S. Li, and X. Luo, "Using quadratic interpolated beetle antennae search to enhance robot arm calibration accuracy," *IEEE Robot. Autom. Lett.*, vol. 7, no. 4, pp. 12046–12053, Oct. 2022.

[73] Z. Li, S. Li, O. O. Bamasag, A. Alhothali, and X. Luo, "Diversified regularization enhanced training for effective manipulator calibration," *IEEE Trans. Neural Netw. Learn. Syst.*, early access, Mar. 9, 2022, doi: 10.1109/TNNLS.2022.3153039.

[74] A. H. Khan, S. Li, and X. Luo, "Obstacle avoidance and tracking control of redundant robotic manipulator: An RNN-based metaheuristic approach," *IEEE Trans. Ind. Informat.*, vol. 16, no. 7, pp. 4670–4680, Jul. 2020.

[75] Z. Li, S. Li, A. Francis, and X. Luo, "A novel calibration system for robot arm via an open dataset and a learning perspective," *IEEE Trans. Circuits Syst. II, Exp. Briefs*, vol. 69, no. 12, pp. 5169–5173, Dec. 2022.

[76] X. Luo, Z. Wang, and M. Shang, "An instance-frequency-weighted regularization scheme for non-negative latent factor analysis on high-dimensional and sparse data," *IEEE Trans. Syst., Man, Cybern., Syst.*, vol. 51, no. 6, pp. 3522–3532, Jun. 2021.

[77] S. Li, J. He, Y. Li, and M. U. Rafique, "Distributed recurrent neural networks for cooperative control of manipulators: A game-theoretic perspective," *IEEE Trans. Neural Netw. Learn. Syst.*, vol. 28, no. 2, pp. 415–426, Feb. 2017.

[78] S. Li, Y. Zhang, and L. Jin, "Kinematic control of redundant manipulators using neural networks," *IEEE Trans. Neural Netw. Learn. Syst.*, vol. 28, no. 10, pp. 2243–2254, Oct. 2017.

Zhibin Li received the B.S. degree in measuring and control technology and instrumentations and the M.E. degree in instrument science and technology from Southwest Petroleum University, Chengdu, China, in 2014 and 2018, respectively. He is currently pursuing the Ph.D. degree in computer science with the Chongqing University of Posts and Telecommunications United training by the Chongqing Institute of Green and Intelligent Technology, Chinese Academy of Sciences, Chongqing, China.

His research interests include robot calibration, big data analysis, and algorithm design for large-scale data applications.

Shuai Li (Senior Member, IEEE) received the B.E. degree in precision mechanical engineering from the Hefei University of Technology, Hefei, China, in 2005, the M.E. degree in automatic control engineering from the University of Science and Technology of China, Hefei, in 2008, and the Ph.D. degree in electrical and computer engineering from the Stevens Institute of Technology, Hoboken, NJ, USA, in 2014.

He is currently a Full Professor with the Faculty of Information Technology and Electrical Engineering, University of Oulu, Oulu, Finland. His current research interests include dynamic neural networks, robotics, machine learning, and autonomous systems.

Xin Luo (Senior Member, IEEE) received the B.S. degree in computer science from the University of Electronic Science and Technology of China, Chengdu, China, in 2005, and the Ph.D. degree in computer science from Beihang University, Beijing, China, in 2011.

He is currently a Professor of data science and computational intelligence with the College of Computer and Information Science, Southwest University, Chongqing, China. He has authored or coauthored over 200 articles (including over 100 IEEE Transactions articles) in the areas of his interests. His research interests include big data analysis and graph learning.

Dr. Luo was a recipient of the Outstanding Associate Editor Award from IEEE/CAA JOURNAL OF AUTOMATICA SINICA in 2020. He is also serving as a Deputy-Editor-in-Chief for IEEE/CAA JOURNAL OF AUTOMATICA SINICA and an Associate Editor for IEEE TRANSACTIONS ON NEURAL NETWORKS AND LEARNING SYSTEMS. His Google page: https://scholar.google.com/citations?user=hyGlDs4AAAAJ&hl=zh-TW